JOURNAL OF SOLID STATE CHEMISTRY 109, 88–96 (1994)

Pb- and Bi-Based Ferrates of Type 2212

T. Fries,* C. Steudtner,* M. Schlichenmaier,* S. Kemmler-Sack,* T. Nissel,† and R. P. Huebener†

*Institut für Anorganische Chemie der Universität, Auf der Morgenstelle 18, D-72076 Tübingen, Germany; and
†Physikalisches Institut der Universität Tübingen, Lehrstuhl für Experimentalphysik II, Auf der Morgenstelle 14, D-72076 Tübingen, Germany

Received January 22, 1993; accepted June 30, 1993

The extent of Pb → Bi substitution in the series of ferrates of type 2212 is studied by XRD, SEM, EDXA, DC resistivity, DC magnetic susceptibility, and vibrational spectroscopic measurements. It is shown that the 2212 structure has an extended field of stability including a pure Pb representative, $PbSr_4Fe_2O_{9+z}$; a simultaneously Bi/Pb substituted series, $Bi_{3-y}Pb_ySr_2Fe_2O_{9+z}$; and the pure Bi system $Bi_{3-x}Sr_{2+x}Fe_2O_{9+z}$. All compounds are basically antiferromagnetic and semiconducting. However, from the observed discontinuity in the magnetic and electrical properties, combined with important differences in the hole concentration, the absence of a simple scheme of substitution follows. The correlation between hole concentration, crystal structure, and physical properties is discussed.

1. INTRODUCTION

Shortly after the discovery of high T_c superconductivity in the new structural family of stacking polytypes $Bi_2Sr_2Ca_{n-1}Cu_nO_{2n+4+z}$ (1), attempts to prepare the corresponding compounds with other transition metal ions were undertaken. These studies have been successful so far for the transition metal ions Mn, Co, Ni, and especially Fe (2, 3). Investigations of the crystal structure (4–10) and physical properties (11–14) of the latter series revealed some significant differences to the Bi-based cuprate, which have their origin in the predominant trivalence of Fe. Consequently, within the whole family the Fe atoms are octahedrally coordinated, thus resulting in an increase of the total oxygen content for $n > 1$ from O_{2n+4+z} (cuprates) to O_{3n+3+z} (ferrates). Similarly to the case of Bi-based cuprates, the structure of the ferrates is stabilized by a partial substitution of Pb for Bi, resulting in the formation of a complete series $(Bi, Pb)_2Sr_2Bi_{n-1}Fe_nO_{3n+3+z}$ with $n = 1$ to 4 (2201 (8, 10), 2212 (5), 2223 (6), and 2234 (7)), in addition to a representative of a new family of stacking polytypes of type 3212 (15). Interestingly, in contrast with the cuprate family, all stacking polytypes with the transition metal ions Mn, Fe, Co, and Ni belong to the class of semiconductors.

The present investigation studies the extent of Pb → Bi substitution in the Fe series of the type 2212 and its influence on the physical properties. It is shown that the 2212 structure has an extended field of stability including a pure Pb representative, $PbSr_4Fe_2O_{9+z}$ (a corresponding composition is unknown in the cuprate 2212 system); a simultaneous Bi/Pb substituted series, $Bi_{3-y}Pb_ySr_2Fe_2O_{9+z}$; and the pure Bi series with a range of composition around $Bi_{3-x}Sr_{2+x}Fe_2O_{9+z}$. However, from the observed discontinuity in the electrical conductivity (relatively low resistivity of $\rho_{RT} \approx 5 \times 10^1\ \Omega$ cm for the pure Bi and Pb end members and nearly insulating regime ($\rho_{RT} \approx 5 \times 10^5\ \Omega$ cm) for the simultaneous presence of Bi and Pb (e.g., $Bi_{2.5}Pb_{0.5}Sr_2Fe_2O_{9.35}$)) and the magnetic properties (variation of the Néel temperature from about 40 K (pure Pb and Bi system) to about 510 K (for simultaneous presence at Bi/Pb)), combined with important differences in the hole concentration, the absence of a simple scheme of substitution follows. It is shown that strong fluctuations in the occupancy and distribution of Sr, Bi, and/or Pb between the rock-salt-like layers and the perovskite slabs, accompanied by significant variations of the overall ionic charge of Bi, Pb, and Fe, are responsible for the observed differences in the physical properties.

2. EXPERIMENTAL

Samples of nominal 2212 composition $(Bi, Pb, Sr)_2(Sr, Bi)_3Fe_2O_{9+z}$ were prepared from $Bi(NO_3)_3 \cdot 5H_2O$ (DAB6, Merck), PbO and $Sr(NO_3)_2$ (p.A., Merck), and Fe (carbonyl-Fe, CS, BASF); in some cases (indicated in Table 1 with an asterisk) between 3 and 5% NaCl and/or NaF was added as flux. The materials were mixed in an agate mortar, and after the decomposition of the nitrates (2 hr/700°C) they were heated in corundum crucibles (Degussit A123) in air to between 960 and 1000°C. The reaction was interrupted several times for regrinding and X-ray analysis (Philips powder diffractometer, Cu$K\alpha$ radiation, Au standard). The heat treatment was stopped after no further change was observed in the XRD. This stage was reached after total reaction times of 100 hr (without flux) or 50 hr (with flux). All samples were air quenched. The materials were characterized by XRD, SEM, EDXA, DC resistivity

0022-4596/94 $6.00

TABLE 1

Lattice Constants (Å[a]), c/a Ratio, Volume of the Tetragonal Subcell V (Å^3), Oxygen Content O_z (Calculated for the Fixed Valences Bi^{3+}, Pb^{2+}, and Fe^{3+}), Average Oxidation State ($\overline{Ox}$) of Bi, Pb, and Fe, Hole Concentration h^+/Formula Unit (Excess of Positive Charge above the Distribution Pb^{2+}, Bi^{3+}, and Fe^{3+}, Calculated from $\overline{Ox}$), and RT Resistivity ρ_{RT} (Ω cm)

Composition[b,c]	a (Å)	c (Å)	c/a	V (Å^3)	O_z	$\overline{Ox}_{Bi,Pb,Fe}$	h^+/formula unit	ρ_{RT} (Ω cm)
				System Pb–Sr–Fe–O				
$PbSr_4Fe_2O_{9.05}$	3.833	30.67	8.00	450.60	$O_{8.00}$	+3.37	2.10	4.8×10^1
$PbSr_4Fe_2O_{9.03}$*	3.840	30.66	7.98	452.10	$O_{8.00}$	+3.35	2.06	2.0×10^1
				System Bi–Sr–Fe–O				
$Bi_{2.75}Sr_{2.25}Fe_2O_{9.48}$*	3.886	31.29	8.05	472.51	$O_{9.38}$	+3.05	0.20	1.9×10^3
$Bi_{2.5}Sr_{2.5}Fe_2O_{9.38}$	3.884	31.63	8.14	477.15	$O_{9.25}$	+3.06	0.26	2.4×10^2
$Bi_{2.5}Sr_{2.5}Fe_2O_{9.39}$*′	3.874	31.45	8.12	472.00	$O_{9.25}$	+3.06	0.28	1.2×10^2
$Bi_{2.25}Sr_{2.75}Fe_2O_{9.32}$*	3.869	31.68	8.19	474.22	$O_{9.13}$	+3.09	0.38	2.8×10^1
				System Bi/Pb–Sr–Fe–P				
$Bi_{2.5}Pb_{0.5}Sr_2Fe_2O_{9.35}$	3.901	31.49	8.07	479.21	$O_{9.25}$	+2.94	0.10	4.5×10^5
$Bi_{2.25}Pb_{0.75}Sr_2Fe_2O_{9.18}$	3.896	31.45	8.07	477.37	$O_{9.13}$	+2.87	0.10	3.4×10^5
$Bi_2PbSr_2Fe_2O_{9.07}$	[d]	31.45	8.10[e]	473.95	$O_{9.00}$	+2.83	0.14	5.0×10^4

[a] ±0.005 (a); ±0.05 (c).
[b] The oxygen content is calculated with the observed $\overline{Ox}_{Bi,Pb,Fe}$.
[c] Samples prepared by using a flux are marked with an asterisk.
[d] Orthorhombic: a = 5.472; b = 5.508 Å.
[e] $2\sqrt{2}c/(a + b)$.

(standard four-probe method), DC susceptibility (SQUID) measurements, IR and FIR spectra, and redox titration for the determination of the oxygen content via the average oxidation state of the cations (16).

3. RESULTS AND DISCUSSION

3.1. XRD, SEM, and EDXA Investigations

Ferrates of type 2212 exist simultaneously in the Bi-free system Pb–Sr–Fe–O, the Pb-free system Bi–Sr–Fe–O, and the partially Pb/Bi-substituted region (Bi/Pb–Sr–Fe–O); some of the latter compounds were first reported in (5).

3.1.1. System Pb–Sr–Fe–O. The pure Pb compound, having no counterpart in the cuprate series, has the composition $PbSr_4Fe_2O_{9+z}$. The phase crystallizes tetragonally and is obtained without impurity phases as by-products by the use of flux, whereas with a conventional solid state route a small admixture of impurity phases (mainly of the Sr_2PbO_4 type) is detectable by XRD (Fig. 1). However, the method of preparation does not influence either the lattice constants or the oxygen content within the limit of experimental error (Table 1). The total composition of the black compound is confirmed by EDXA, with a resulting value of $Pb_{0.91}Sr_{4.11}Fe_2O_y$. The material has a mica-like platy texture, very familiar to the series of Bi-based cuprates. Figure 2 gives a SEM image of the surface of a pellet of composition $PbSr_4Fe_2O_{9.05}$. The preferred orientation, with the c-axis normal to the surface plane, is likewise observed in the XRD pattern of pressed pellets by the strong increase in the intensity of 001 reflections.

From the observed average oxidation state of Pb and Fe ($\overline{Ox}_{Pb,Fe}$ = +3.35), the presence of an exceptionally high hole concentration h^+/formula unit follows. According to the observed physical properties (cf. Sections 3.2. and 3.3.) the holes are predominantly localized. Likewise, a valence of +4.05 for either Pb or Fe can be calculated by assuming the simultaneous presence of either Fe^{3+} or Pb^{2+}. Taking into account that Fe^{4+} in its high spin state $t_{2g}^3 e_g^1$ is a Jahn–Teller ion, the presence of elongated FeO_6 octahedra having their long axis is the c direction of the 2212 structure is anticipated. Consequently, the content of high spin Fe^{4+} should be expressed by an exceptionally high ratio for c/a. However, a comparison of the c/a values of the 2212 ferrates in Table 1 gives quite the opposite result, thus ruling out the presence of larger amounts of high spin Fe^{4+}. In combination with the observed electrical properties (cf. Section 3.3), electron hopping between Fe^{3+} and Fe^{4+} on identical octahedral sites can be assumed, resulting in an intermediate valence state between them. This situation is likewise realized in ferrate perovskites of the type $La_{1-x}A_xFeO_{3-y}$ (A = Ba, Sr (17)). Moreover, the observed reduced c/a value, in combination with the relatively small volume of the unit cell (compared with the values for the Bi-containing series; Table 1), can be interpreted by the presence of Pb^{4+}

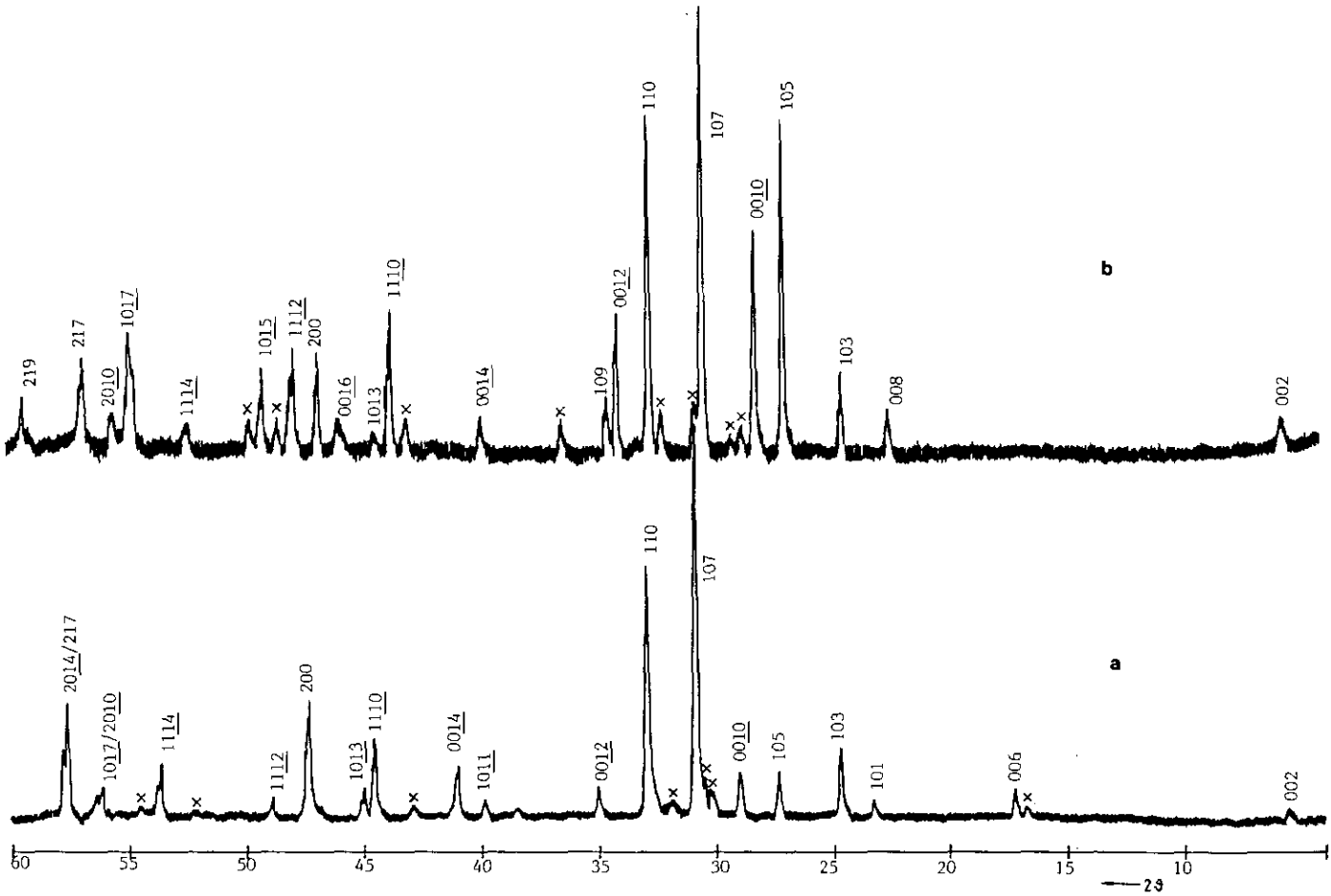

FIG. 1. Section of the XRD pattern for flux-free preparations of powdered samples of composition (a) $PbSr_4Fe_2O_{9.05}$ and (b) $Bi_{2.5}Sr_{2.5}Fe_2O_{9.39}$. The reflections of the 2212 phase are indicated; the impurity phases are marked by crosses.

with its relatively small ionic radius (0.775 Å; CN 6 (18)) in comparison with the values of Pb^{2+} (1.19 Å), Bi^{3+} (1.03 Å), and Sr^{2+} (1.18 Å). The observed oxygen content is within the limit of experimental error, in agreement with the ideal value $O_{9.00}$ of type 2212. Therefore, the presence of a modulated superstructure, based on the insertion of oxygen in the rock-salt-like layers is very unlikely.

Structural calculations were performed from XRD data of flux-free prepared $PbSr_4Fe_2O_9$ for the space group I4/*mmm* according to the results for the 2212 ferrate $Bi_{2.5}Pb_{0.5}Sr_2Fe_2O_{9+z}$ (5). With the refined atomic positions of Table 2 the reliability factor, $R_{int} = \Sigma |I_0 - I_c|/\Sigma I_c$, is 12.3%. The observed and calculated intensities are summarized in Table 3. From these results the validity of the 2212 structure for $PbSr_4Fe_2O_9$ is confirmed. The Pb atoms (Pb(1)) occupy exclusively the rock-salt-like layers in combination with a similar amount of Sr (Sr(1)). From the observed occupancy values of Pb(1) and Sr(1) a slight deficiency in Pb results, most probably indicative of a minor Pb loss due to volatilization. This observation is in agreement with the EDXA data. Correspondingly, the Pb deficiency was compensated for by Sr. In the perovskite slabs, in addition to the iron atoms, only Sr (Sr(2) and (3)) is found. Whereas the sites of Fe and Sr(3) are completely filled, for the position of Sr(2) a deficiency of 25% is observed. Furthermore, an unexpected high temperature factor $B = 2.0$ for the oxygen atoms O(2) in the same Sr(2)–O(2) layer is indicative of disorder and/or additional atomic displacements within the x/y plane. In the latter direction points the extremely short Fe–O(2) distance of 1.17 Å in comparison with the values of 1.95 and 2.29 Å for Fe–O(1) and Fe–O(4), which fall within the usual range. Although not very accurate due to the low oxygen scattering factor, the observed variations in the Fe–O distances along the c direction (Fe–O(2) and Fe–O(4)) are extreme compared to the corresponding values for the 2212 ferrate $Bi_{2.5}Pb_{0.5}Sr_2Fe_2O_9$ (5) of 1.80, 1.67, and 1.96 Å for Fe–O(2), Fe–O(4), and Fe–O(1); this is most probably indicative of a tilting of the FeO_6 octahedra in the present pure Pb compound. Another pronounced difference between the structure of $Bi_{2.5}Pb_{0.5}Sr_2Fe_2O_9$ and that of $PbSr_4Fe_2O_9$ consists in the reduction of the distance

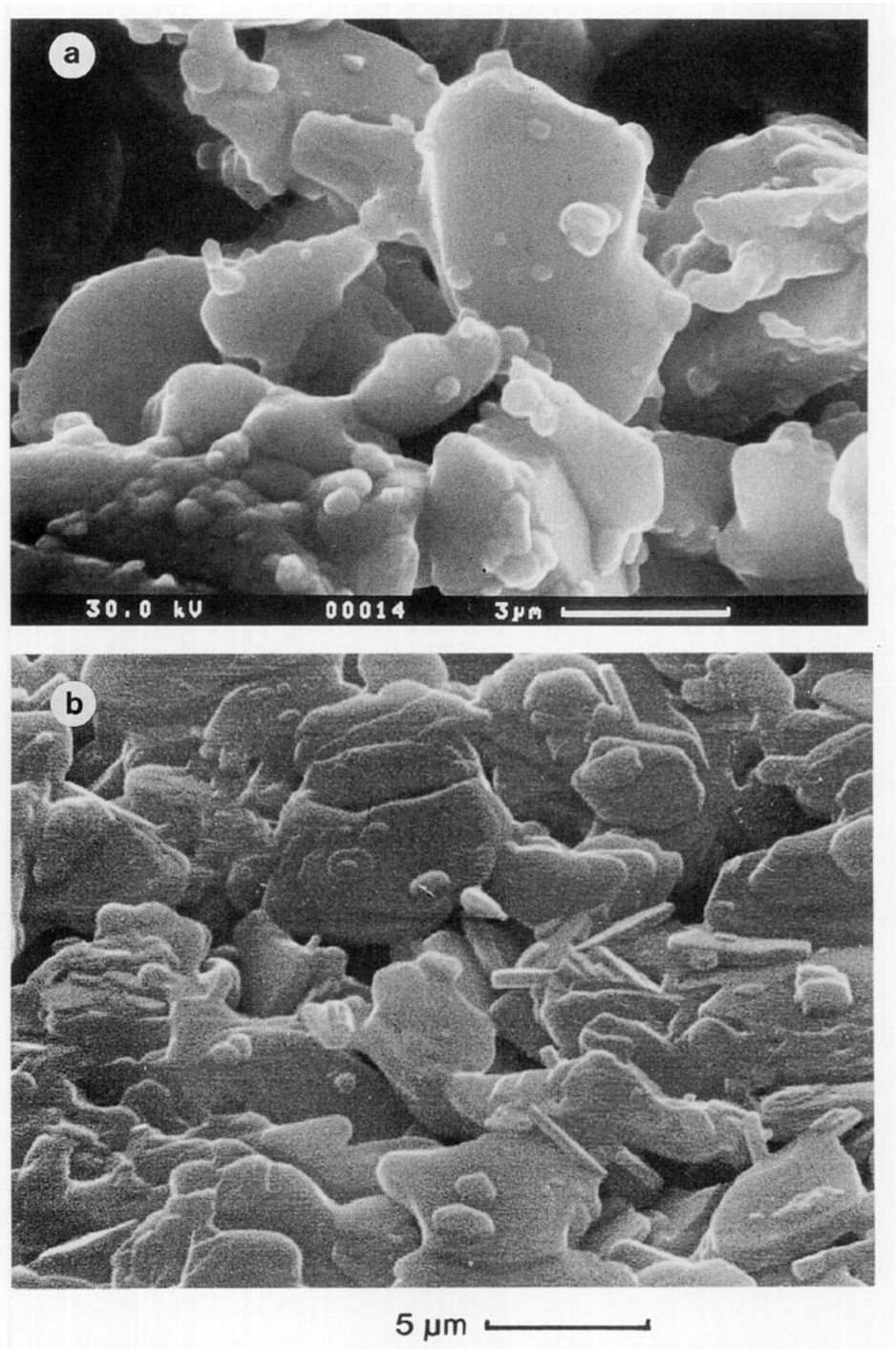

FIG. 2. SEM of the surface of a pellet of (a) $PbSr_4Fe_2O_{9.05}$ and (b) $Bi_{2.5}Sr_{2.5}Fe_2O_{9.39}$.

between the two rock-salt-like layers from 5.56 to 5.02 Å. From a detailed comparison of the cation oxygen distances of 2.04 Å for Pb(1)/Sr(1)–O(3) or 3.01 Å for Bi(1)/Pb(1)–O(3), and 2.62 Å for Sr(2)–O(3) or 2.55 Å for Sr(1)/Bi(2)–O(3), it follows that the reduced extension of the Sr(1)/Pb(1)–O layer is responsible for the observed shrinkage; this is easily explainable by the anticipated presence of Pb^{4+} (see above).

3.1.2. System Bi–Sr–Fe–O. For the pure bismuth ferrate the ideal composition $Bi_2Sr_3Fe_2O_{9.00}$ is expected (19–21). However, we have been unable to prepare homogeneous materials of this composition by using either different solid state routes or several fluxes. From numerous experimental results it follows that the pure bismuth ferrate has a range of composition around the Bi-rich formula $Bi_{3-x}Sr_{2+x}Fe_2O_{9+z}$. The phase boundaries were deter-

TABLE 2
$PbSr_4Fe_2O_9$: Atomic Coordinates and Isotropic Thermal Displacement Parameters B (Å^2) Refined from Powder XRD Data

Atom	Site	x	y	z	Occupancy	B
Pb(1)	4*e*	0	0	0.2940	0.45	0.0
Sr(1)	4*e*	0	0	0.2940	0.55	0.0
Sr(2)	4*e*	0	0	0.1305	0.75	1.0
Sr(3)	2*a*	0	0	0	1.00	0.0
Fe	4*e*	0	0	0.4255	1.00	0.5
O(1)	8*g*	0.5	0	0.4365	1.00	0.0
O(2)	4*e*	0	0	0.3875	1.00	2.0
O(3)	4*e*	0	0	0.2160	1.00	0.0
O(4)	2*b*	0	0	0.5	1.00	0.0

Note. Space group $I4/mmm$; $R_{int} = \Sigma |I_o - I_c|/\Sigma I_c = 12.3\%$.

mined in steps of $0.25x$, where $0.25 \leq x \leq 0.75$. For the synthesis, the solid state route and the flux method were simultaneously employed. The latter results in completely homogenous materials, whereas in the former case a small admixture of impurity phases (mainly a perovskite phase of type (Sr, Bi)–(Fe, Bi)O_{3+z}) is observed in the XRD (Fig. 1). Similar to the pure Pb system neither the lattice constants nor the analytical data are meaningfully influenced by the method of preparation. All members of the pure Bi series are black and crystallize tetragonally (Table 2), and the observed extinctions are in agreement with the space group $I4/mmm$. With decreasing Bi content the lattice constant a is slightly reduced, whereas the c-axis expands. In the same direction the average oxidation state of Bi and Fe goes slightly up. However, the total oxygen content decreases, demonstrating that the increase of $\overline{Ox}_{Bi,Fe}$ is overcompensated for by the simultaneous reduction of the content of Bi. Nevertheless, an excess of oxygen is present within the entire series, indicating the possible development of a modulation within the rock-salt-like layers, due to the insertion of the additional oxygen atoms. In the pure Bi system an excess of positive charge (h^+/unit cell) is present, localized on either the cations or the oxygen anion. The latter situation was recently observed in the system $La_{1-x}Sr_xFeO_3$ (22).

TABLE 3
Observed (I_o) and Calculated Intensities (I_c) for $PbSr_4Fe_2O_9$

h	k	l	I_o	I_c	h	k	l	I_o	I_c
0	0	2	24	44	1	0	15	0	12
0	0	4	0	24	2	0	6	0	0
0	0	6	50	5	2	0	8	0	5
0	0	8	18	24	1	2	1	0	1
1	0	1			2	1	1		
1	0	3	151	148	0	0	18	185	191
1	0	5	86	87	1	1	14		
0	0	10	111	109	1	2	3		
1	0	7	983	1000	2	1	3		
1	1	0	607	630	1	2	5	10	32
1	1	2	8	65	2	1	5		
0	0	12	70	50	1	0	17	151	152
1	1	4			2	0	10		
1	0	9			1	2	7	328	332
1	1	6	0	14	2	1	7		
1	0	11	28	15	1	1	16	10	5
1	1	8	8	7	0	0	20	46	32
0	0	14	157	126	2	0	12		
1	1	10	225	218	2	1	9		
1	0	13	70	10	1	2	9		
0	0	16	332	328	1	0	19	28	18
2	0	0			1	2	11	12	5
2	0	2	0	4	2	1	11		
1	1	12	40	68	1	1	18	129	122
2	0	4			2	0	14		

The compounds of the Bi series are characterized by a platy, mica-like texture, similar to that of the pure Pb (see above) or the Bi/Pb-substituted system (5). Figure 2 shows a SEM image of a surface of a pellet of composition $Bi_{2.5}Sr_{2.5}Fe_2O_{9.39}$. The preferred orientation of crystallites, a typical behavior of Bi-based stacking polytypes with the c-axis lying normal to the surface plane, is likewise expressed by the huge increase of the 001 reflections in the XRD pattern of pressed pellets.

3.1.3. System Bi/Pb–Sr–Fe–O. The composition of the members of the partially Pb → Bi-substituted system can be expressed by the general formula $Bi_{3-y}Pb_ySr_2Fe_2O_{9+z}$. Thus, the observed composition is directly correlated to the pure Bi–Sr–Fe–O system ($Bi_{3-x}Sr_xSr_2Fe_2O_{9+z}$; cf. Section 3.1.2) and confirms likewise the nonexistence of a hypothetical Sr-rich composition $(Bi, Pb)_2Sr_3Fe_2O_9$, even in the case of Pb substitution. Similar to the pure Bi system in the Bi/Pb series, the 2212 structure needs stabilization; it is stabilized by a partial substitution of Bi by Pb, whereas for the pure Bi system Sr is used. For a small substitution rate ($y \leq 0.75$) the unit cell is tetragonal; however, for $y = 1.0$ a small orthorhombic distortion takes place (Table 1). The average oxidation state of Bi, Pb, and Fe is always below +3 and decreases with increasing Pb content. Note that the total oxygen content only slightly exceeds the calculated value of O_z. Consequently, the real charge distribution is near the assumed fixed values of Bi^{3+}, Pb^{2+}, and Fe^{3+} for the calculation of O_z, and the hole concentration is low. In the same direction points the relatively high electrical resistivity (cf., Section 3.3) in combination with the observed dark reddish color of the Bi/Pb–Sr–Fe–O system. This coloration is in contrast with the black color of the pure Pb and Bi series. From the diffuse reflectance spectra of the Bi/Pb series a band gap of about 2 eV is calculated, a typical value for antiferromagnetically ordered iron oxides (23).

Contrary to the pure Pb system, the rock-salt-like layers are exclusively occupied by Bi and Pb (not distinguishable

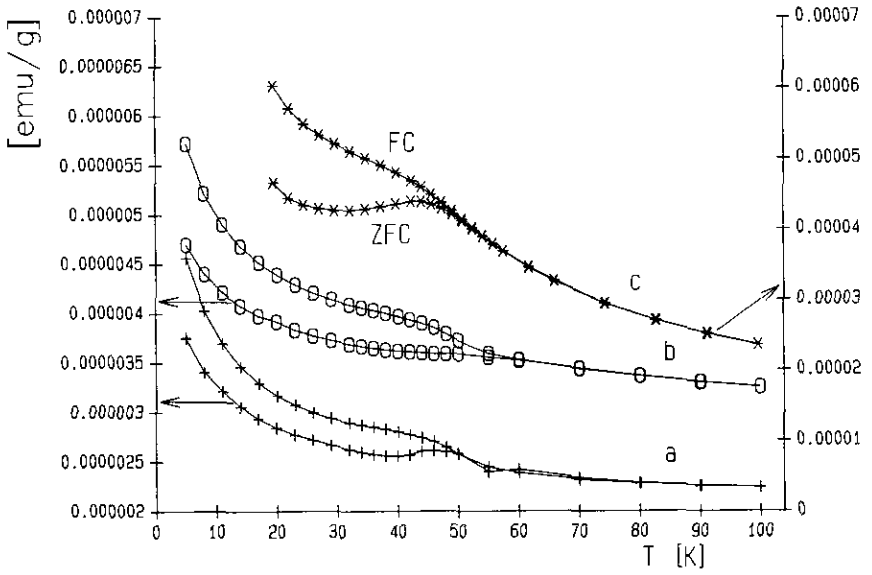

FIG. 3. χ vs T in the range 5–100 K. (a) $Bi_{2.25}Sr_{2.75}Fe_2O_{9.32}$, (b) $Bi_{2.75}Sr_{2.25}Fe_2O_{9.48}$, and (c) $PbSr_4Fe_2O_{9.03}$.

by X-rays due to the identical scattering factors). Interestingly, the remaining Bi/Pb and the Sr atoms do not have an orderly distribution over the sites 2*a* (between the FeO_6 octahedra) and 4*e* (at linkage between the rock-salt and perovskite slabs) but are present purely statistically on both positions in the ratio 2 : 1 (5).

3.2. *Magnetic Properties*

The temperature dependence of the magnetic susceptibility was measured after pellets of the 2212 materials were cooled in zero field (ZFC) from room temperature (RT) to 5 K. Then a field of 0.1 T for $PbSr_4Fe_2O_{9+z}$ and 1.0 T for the series $Bi_{2-x}Sr_{2+x}Fe_2O_{9+z}$ was applied while they were warmed to 300 K. Without changing the field the measurement was performed by cooling the sample in a field (FC). Some examples are shown in Fig. 3.

In the ZFC regime for all samples a maximum is observed around 30–50 K. For all compounds the magnetization in the FC regime is larger than in the ZFC one. The irreversibility starts around the temperature where the maximum occurs. From the observed temperature dependence one can conclude that the materials are basically antiferromagnetic with Néel temperatures corresponding to the irreversibilities in the FC regime. Additionally, the observed small variations of T_N within the Bi system $Bi_{3-x}Sr_{2+x}Fe_2O_{9+z}$ reveals the absence of meaningful fluctuations in the valence state of Fe. This finding is in agreement with the observed, nearly constant average oxidation state $\overline{Ox}$.

Many aspects of the observed magnetic behavior of the pure lead and bismuth ferrates of type 2212 resemble those of the analog Fe-based stacking polytypes of type 2201 Bi $PbFe_{1-x}M_xO_{6+z}$ (M = Co, Ni (11)), likewise basically characterized as antiferromagnets without sharp peaks in the temperature dependence of the susceptibility. For single crystals of $BiPbSr_2MnO_6$ a similar observation was recently explained by the lack of structural modulation (24).

For the 2212 materials of the Bi/Pb series, $(Bi_{2-x}Pb_x)Sr_2BiFe_2O_{9+z}$, the magnetic properties were studied by Mössbauer spectroscopic measurements for $x = 0.5$ (12). It is shown that the material is likewise antiferromagnetic. However, in contrast with the pure Pb and Bi systems, the Néel temperature is situated at 512 K, significantly above RT. The valence of Fe is mainly +3.

Most likely, the reduced number of charge carriers (h^+/formula unit in Table 1), combined with their low mobility (cf. Section 3.3), is responsible for the increase of T_N in the Bi/Pb system. The pure Pb and Bi systems with a higher number of holes are characterized by an enforced hopping conductivity. Consequently, for charge localization, an important condition for the development of antiferromagnetism, a decrease of temperature to much lower values than in the Bi/Pb case is necessary.

3.3. *Electrical Properties*

According to the analytical investigations all ferrates of type 2212 contain an excess of positive charge carriers (h^+/unit cell; Table 1). From the measurement of the temperature dependence of the electrical resistivity it follows that uniform semiconductivity is present (Fig. 4). However, for a fixed temperature the values of ρ vary by about a factor of 10^4. For demonstration the ρ_{RT} values are indicated in Table 1. As with the smallest values of h^+/unit cell, the highest resistivity is present for the simultaneous incorporation of Bi and Pb (series Bi/Pb–Sr–Fe–O). The pure Pb and the pure Bi systems are characterized by significantly lower values due to the higher hole concentration.

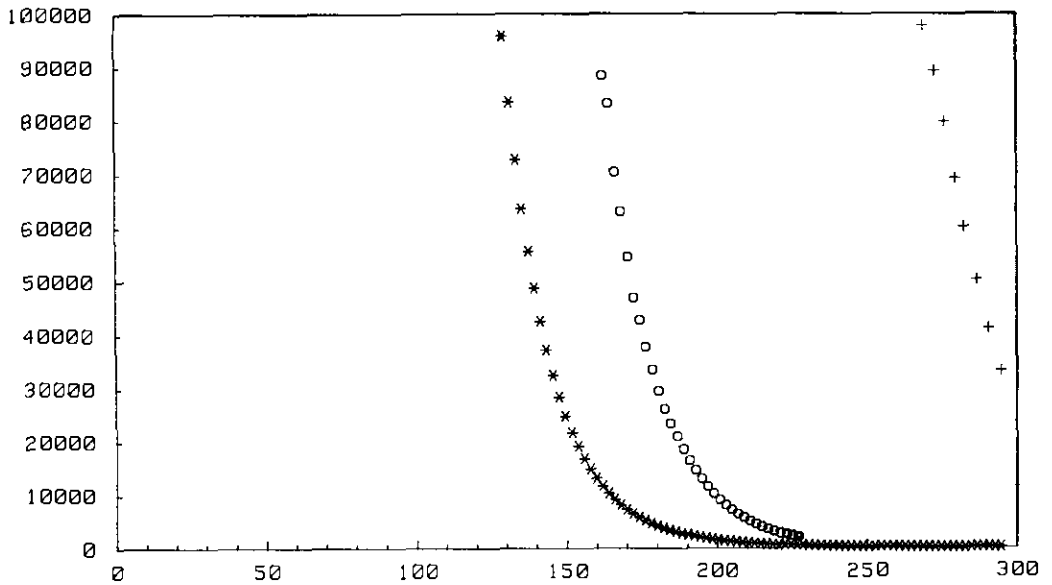

FIG. 4. ρ vs T for (*) $PbSr_4Fe_2O_{9.05}$, (○) $Bi_{2.25}Sr_{2.75}Fe_2O_{9.32}$, and (+) $Bi_2PbSr_2Fe_2O_{9.07}$.

From a plot of ln ρ vs $1/T$ it follows that all ferrates deviate from Arrhenius behavior. Consequently, no simple thermally activated process is present over the whole temperature region. However, for smaller sections the observed temperature dependence can be approximated by $\rho = \rho_0\, e^{-E_a/kT}$. For the activation energy E_a of $PbSr_4Fe_2O_{9.05}$, values between 0.12 eV (130–160 K) and 0.18 eV (170–295 K); for $Bi_{2.25}Sr_{2.75}Fe_2O_{9.32}$, between 0.17 eV (170–190 K) and 0.21 eV (200–240 K); and for $Bi_2PbSr_2Fe_2O_{9.07}$, between 0.13 eV (240–255 K) and 0.14 eV (270–285 K) have been found. Attempts to fit the temperature variation of the resistivity by the form $\rho = \exp(T_0/T)^{1/n}$ with $n = 2$–4 also failed within the whole temperature region. Similar behavior was observed for ferrates of the type 2201 (2).

Analysis of the resistivity measurements indicates that the main difference between the Bi/Pb series and the pure Pb or pure Bi system is based on the reduced number of h^+ in the former. Consequently, for the pure Bi system the smaller values of ρ are combined with an increase of h^+/unit cell. However, for the pure Pb compound an additional decrease of ρ should be expected by considering the high value of h^+/unit cell. From the absence of this effect it follows that the holes are predominantly localized (as Pb^{4+}).

3.4. *Infrared Spectra*

The infrared spectra are analyzed on the basis of the spectroscopic unit cell for ferrates of the 2212 type (space group $I4/mmm - D_{4h}^{17}$ (atomic positions in Table 2) with one formula unit $A_2B_2MFe_2O_9$. Factor group analysis (25) leads, with $k = 0$, to the total amount of irreducible representations

$$\Gamma_{tot} = 6A_{1g} + B_{1g} + 7E_g + 8A_{2u} + B_{2u} + 9E_u$$

(including the translations $A_{2u} + E_u$).

For the ferrates of the 2212 type, well-developed infrared spectra are observed, in agreement with the semiconducting properties of the materials. Metallic conductors are characterized by a continuous absorption (26, 27). From the expected 12 IR-active vibrations $7A_{2u}$ and $8E_u$ a maximum of eight bands can be separated in the Bi–Sr–Fe–O and Bi/Pb–Sr–Fe–O systems, denoted as ν_1–ν_8 and listed in Table 4. Some examples are given in Fig. 5. From a comparison with the vibrational spectroscopic data of other perovskite oxides (28) it follows that the higher-energetic frequencies ν_1–ν_3 are typical of vibrations within the framework of FeO_6 octahedra, whereas the lattice modes of the heavier atoms Sr and Bi are situated at lower frequencies (ν_4–ν_8). For the Bi-containing systems Bi–Sr–Fe–O and Bi/Pb–Sr–Fe–O the position of the vibrational modes ν_1–ν_8 is practically conserved. Consequently, their crystal structures are deduced to be very similar. In the pure Pb system a significant shift of ν_1, ν_2, and ν_3, assigned predominantly as vibrations within the FeO_6 framework, is present, thus indicating modifications in the bonding system of the 2212 structure due to the higher hole concentration. In agreement with the results of the structure determination, the magnetic and electrical measurements suggest that the holes are predominantly localized in the form of Pb^{4+}. In the case of a hole localization at Fe^{4+} a higher energetic

TABLE 4
IR/FIR Vibration Modes (cm^{-1})[a]

Composition	ν_1	ν_2	ν_3	ν_4	ν_5	ν_6	ν_7	ν_8
$PbSr_4Fe_2O_{9.05}$	670	595	430		⟵ b ⟶		180	90
$Bi_{2.75}Sr_{2.25}Fe_2O_{9.48}$	720	605	470	390sh	300b	230sh	175	105
$Bi_{2.5}Sr_{2.5}Fe_2O_{9.38}$	720	605	475	390sh	300b	240sh	175	105
$Bi_{2.25}Sr_{2.75}Fe_2O_{9.32}$	710	605	475	—	300b	240sh	180	110
$Bi_{2.5}Pb_{0.5}Sr_2Fe_2O_{9.35}$	715	600	470	390sh	290b	225	160	130sh

[a] sh = shoulder, b = broad.

shift of ν_1–ν_3 is expected as a consequence of a covalence of the Fe^{4+}–O bond, which is stronger than that of the Fe^{3+}–O bond. In the region ν_4–ν_6 ill-resolved broad bands are observed due to strong coupling between the lattice modes as a result of the simultaneous occupancy of the sites 4*e* and 2*a* by Sr atoms.

4. CONCLUSIONS

Ferrates of the 2212 type show an extended field of stability for Pb → Bi substitution, including a pure Bi series $Bi_{3-x}Sr_{2+x}Fe_2O_{9+z}$, Bi/Pb substituted materials $Bi_{3-x}Pb_xSr_2Fe_2O_{9+z}$, and a pure Pb compound $PbSr_4Fe_2O_{9+z}$. For the structurally strongly related superconducting 2212 cuprates $Bi_{2-x}Pb_xSr_2CaCu_2O_{8+z}$ a similar extended range of composition is unknown, attaining a maximum Pb content of $x \approx 0.6$ (29). Consequently, for Bi- and Bi/Pb-based ferrates and cuprates in the rock-salt-like layers between the perovskite slabs mainly Bi and some Pb are likewise present. However, in case of ferrates there exists a second possibility, exclusive occupancy by Pb and Sr. Moreover, additional important differences between ferrates and cuprates consist in the predominant trivalence of Fe, which is exclusively octahedrally coordinated by oxygen, in contrast to a quadratic pyramidal coordination of Cu with an average oxidation state near +2.2. Similarly to the cuprate case, ferrates are characterized by a certain content of holes. However, the charge carriers are predominantly localized, resulting in semiconductivity and antiferromagnetism.

ACKNOWLEDGMENTS

This work was supported by the Bundesministerium für Forschung und Technologie (FKZ 03-KS3TUE) and the Verband der Chemischen

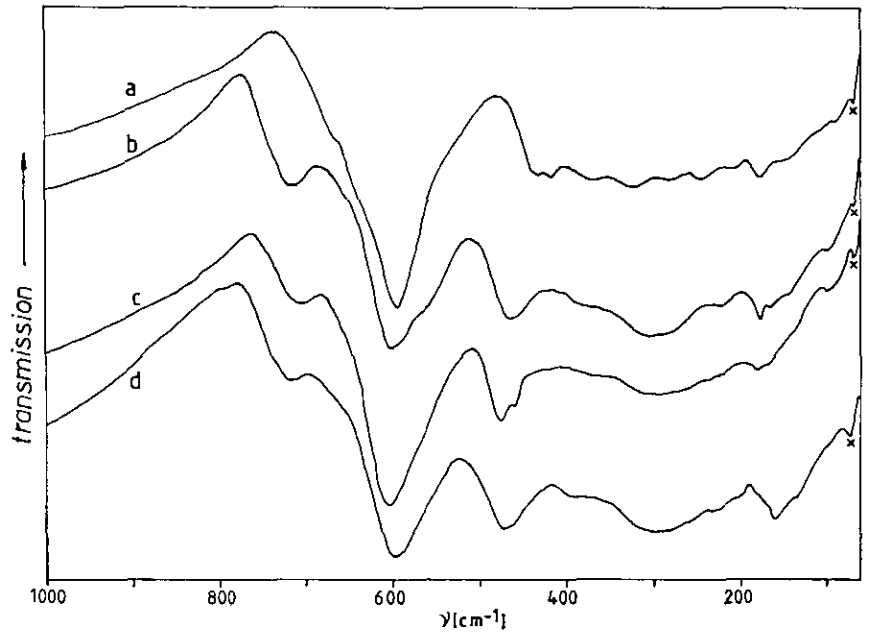

FIG. 5. Infrared spectra of (a) $PbSr_4Fe_2O_{9.05}$, (b) $Bi_{2.75}Sr_{2.25}Fe_2O_{9.48}$, (c) $Bi_{2.5}Pb_{0.5}Sr_2Fe_2O_{9.35}$, and (d) $Bi_{2.5}Sr_{2.5}Fe_2O_{9.38}$; absorption of polyethylene is marked by a cross.

Industrie. The authors thank the BASF AG, Ludwigshafen, for supplying the iron powder. We are indebted to Prof. Dr. E. Lindner and G. Farag for the measurement of the FIR spectra. The help of Mrs. A. Ehmann and Mrs. E. Niquet is much appreciated.

REFERENCES

1. H. Maeda, Y. Tanaka, M. Fukotomi, and T. Asano, *Jpn. J. Appl. Phys.* **27,** L209 (1988).
2. A. Ehmann, T. Fries, S. Kemmler-Sack, S. Lösch, T. Rentschler, M. Rygula, M. Schlichenmaier, and W. Wischert, *J. Less-Common Met.* **164** and **165,** 596 (1990), and the literature cited therein.
3. S. Kemmler-Sack, A. Ehmann, T. Fries, R. Kiemel, S. Lösch, G. Mayer-von Kürthy, and M. Schlichenmaier, *J. Less-Common Met.* **152,** L27 (1989).
4. S. Kemmler-Sack, A. Ehmann, T. Fries, G. Mayer-von Kürthy, S. Lösch, and M. Schlichenmaier, *J. Less-Common Met.* **153,** L31 (1989).
5. T. Fries, G. Mayer-von Kürthy, A. Ehmann, S. Lösch, M. Schlichenmaier, and S. Kemmler-Sack, *J. Less-Common Met.* **153,** L37 (1989).
6. G. Mayer-von Kürthy, T. Fries, A. Ehmann, S. Lösch, M. Schlichenmaier, S. Kemmler-Sack, F. Badel, D. Kölle, and R. P. Huebener, *J. Less-Common Met.* **153,** L43 (1989).
7. T. Fries, G. Mayer-von Kürthy, A. Ehmann, and S. Kemmler-Sack, *J. Less-Common Met.* **154,** L1 (1989).
8. T. Fries, G. Mayer-von Kürthy, A. Ehmann, W. Wischert, and S. Kemmler-Sack, *J. Less-Common Met.* **159,** 337 (1990).
9. A. Ehmann, T. Fries,and S. Kemmler-Sack, *J. Less-Common Met.* **162,** L35 (1990).
10. N. Stüsser, R. Sonntag, D. Hohlwein, Th. Zeiske, A. Hoser, S. Kemmler-Sack, T. Fries, and T. Vogt, *Z. Phys. B: Condens. Matter* **83,** 165 (1991).
11. Th. Sinnemann, M. Mittag, M. Rosenberg, A. Ehmann, T. Fries, G. Mayer-von Kürthy, and S. Kemmler-Sack, *J. Magn. Magn. Mater.* **95,** 175 (1991).
12. Th. Sinnemann, L. Kessler, M. Rosenberg, T. Fries, A. Ehmann, and S. Kemmler-Sack, *J. Magn. Magn. Mater.* **98,** 99 (1991).
13. Y. Watanabe, D. C. Tsui, J. T. Birmingham, N. P. Ong, and J. M. Tarascon, *Phys. Rev.* **43,** 3036 (1991), and the literature cited therein.
14. M. Pissas, A. Simopoulos, A. Kostikas,and D. Niarchos, *Physica C* **176,** 227 (1991).
15. G. Mayer-von Kürthy, T. Fries, A. Ehmann, and S. Kemmler-Sack, *J. Less-Common Met.* **155,** L19 (1989).
16. W. Schäfer, J. Maier-Rosenkranz, S. Lösch, R. Kiemel, W. Wischert, and S. Kemmler-Sack, *J. Less-Common Met.* **142,** L5 (1988).
17. J. Li, X. Cai, and T. H. Wang, *Appl. Phys. A* **55,** 158 (1992).
18. R. D. Shannon, *Acta Crystallogr., Sect. A* **32,** 751 (1976).
19. M. Hervieu, C. Michel, N. Nguyen, R. Retoux, and B. Raveau, *Eur. J. Solid State Inorg. Chem.* **25,** 375 (1988).
20. Y. Le Page, W. R. McKinnon, J.-M. Tarascon, and P. Barboux, *Phys. Rev. B* **40,** 6810 (1989).
21. M. Pissas, A. Kostikas, D. Niarchos, and A. Simopoulos, *J. Less-Common Met.* **164** and **165,** 581 (1990).
22. M. Abbate, F. M. F. de Groot, J. C. Fuggle, A. Fujimori, O. Strebel, F. Lopez, M. Domke, G. Kaindl, G. A. Sawatzky, M. Takano, Y. Takeda, H. Eisaki, and S. Uchida, *Phys. Rev. B* **46,** 4511 (1992).
23. D. M. Sherman and T. D. Waite, *Am. Mineral.* **70,** 1262 (1985).
24. J. M. Tarascon, Y. Le Plage, W. R. McKinnon, R. Ramesh, M. Eibschütz, E. Tselepis, E. Wang, and G. W. Hull, *Physica C* **167,** 20 (1990).
25. D. M. Adams and D. C. Newton, "Tables for Factor Group and Point Group Analysis." Beckman RIIC Ltd., Croydon, England, 1970.
26. E. Beck and S. Kemmler-Sack, *J. Less-Common Met.* **135,** 257 (1987), and the literature cited therein.
27. G. Mayer-von Kürthy, W. Wischert, R. Kiemel, and S. Kemmler-Sack, *J. Solid State Chem.* **79,** 34 (1989).
28. A. Fadini, I. Jooss, S. Kemmler-Sack, G. Rauser, H.-J. Rother, E. Schillinger, H.-J. Schittenhelm, and U. Treiber, *Z. Anorg. Allg. Chem.* **439,** 35 (1978).
29. M. Schlichenmaier and S. Kemmler-Sack, *Physica C* **198,** 175 (1992).